Evaluating the potential for tsunami generation in southern Iran

Mohammad Heidarzadeh[1], Moharram Dolatshahi Pirooz[2], Nasser Hadjizadeh Zaker[3], Mohammad Mokhtari[4]

[1]PhD Candidate of Civil Engineering, College of Engineering, University of Tehran, Tehran, Iran
Email: heidarz@ut.ac.ir
[2]Assistant Professor of Civil Engineering, College of Engineering, University of Tehran, Tehran, Iran
[3]Assistant Professor, Graduate Faculty of Environment, University of Tehran, Tehran, Iran
[4]Assistant Professor, International Institute of Earthquake Engineering and Seismology, Tehran, Iran

Abstract: *Makran Subduction Zone (MSZ) offshore of Iran and Pakistan is one of the most tsunamigenic sources in the Indian Ocean. Historically, the MSZ has generated some tsunamigenic earthquakes like that of 28 November 1945 with the death tool of more than 4000 people along the coasts of Iran, Pakistan, India, and Oman. In this study, the tsunami hazard associated with the MSZ is investigated. At first, a review of historical tsunamis in the Indian Ocean basin was performed which reveals the Makran region has experienced al least 4 tsunamis including events of 326 BC, 1897, 1008, and 1945. Consequently, since the pattern and extent of vertical ground deformation from an earthquake determines whether or not a tsunami is formed, a computer program is developed to predict the seafloor deformation due to the earthquake occurrence in the MSZ. The model was verified through run of it on some actual tsunamis so far occurred. Then, using the data of the 1945 Makran tsunami, the seismic parameters of the MSZ were calibrated. Finally, we used the developed computer program to calculate seafloor deformation at the location of Makran subduction zone for several earthquake scenarios with moment magnitudes ranging between 6.5 and 8.5. The results of this research show that the risk of tsunami generation from MSZ can be classified into three main categories, as follows: (1) very little risk for tsunami generation in the case of the occurrence of an earthquake having magnitude up to 7; (2) little to medium risk for moment magnitudes ranging between 7 and 7.5; and (3) high risk for moment magnitude greater than 7.5. At the end of the paper, modeling of tsunami propagation is performed for an earthquake scenario with magnitude of 8 offshore Chabahar, in order to give preliminary information about tsunami behavior in this region.*

Keywords: *Tsunami, Indian Ocean, Makran Subduction Zone, Tsunami Generation, Tsunami Propagation*

1. Introduction

Tsunamis are gravity long waves generated by impulsive geophysical events of seafloor, volcanoes, asteroid impacts and landslides. However, by far the most common cause is submarine earthquake [1] which owning to its occurrence the earth's crust experiences vertical deformations in the form of uplift and subsidence (Figure 1-A). When seafloor abruptly deforms, the overlaying water will be displaced from its equilibrium position and consequently tsunami waves will be generated due to the effect of gravity (Figure1-B). A review of world tsunami events performed by Synolakis (2003) [1]; Gusiakov (2005) [2]; Gusiakov (2001) [3]; Murty and Rafiq (1991) [4]; Murty and Bapat (1999) [5]; Rastogi and Jaiswal (2006) [6] reveals that tsunamis are not as common in the Indian Ocean as in the Pacific. As compared to average eight tsunamis per year in the Pacific, Indian Ocean has one in three years or so [6].

Hence, prior to the 2004 mega-tsunami,

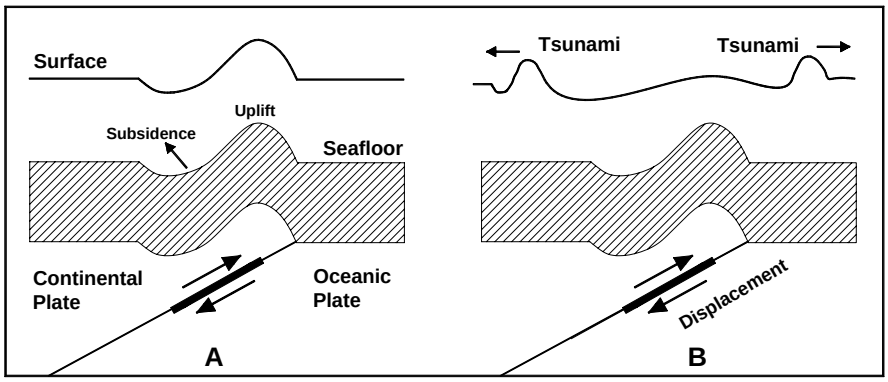

Fig.1 Tsunami generation by underwater earthquakes

considering limited number of tsunami occurrences in the Indian Ocean, the necessity for investigating tsunami hazard and developing tsunami warning systems in this region was disregarded. Nonetheless, following the massive loss of life caused by the Sumatra tsunami in December 2004 in Indonesia, the need for investigating the possibility of tsunami generation in the Indian Ocean basin was further emphasized. Assessment of the historical records of tsunamis in the Indian Ocean by Dominey-Howes et al. (2006) [7]; Murty and Rafiq (1991) [4]; Murty and Bapat (1999) [5] shows that essentially there are two main tsunamigenic zones in this ocean, which are Sunda subduction zone in the east, and Makran subduction zone in the north-west of the Indian Ocean (Figure 2).

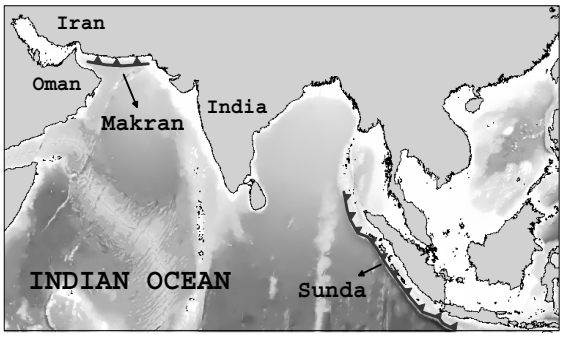

Fig.2 Two main tsunamigenic sources in the Indian Ocean including Sunda and Makran

In the most recent Indian Ocean tsunami catalog, Dominey-Howes et al. (2006) [7] have reported 26 tele-tsunamis in the Indian Ocean basin from 326 BC to 2005 AD. The source zones for these events are the Makran subduction zone off the coast of Iran and Pakistan and the Sunda Arc stretching from the coast of Myanmar through the Andaman and Nicobar Islands and along the Indonesian archipelago. Among these events, 23 events are from Sunda, and 3 from, or near Makran. Based on Rastogi and Jaiswal (2006) [6] Sunda subduction zone is the most active region that has produced about seventy tsunamis. In addition, the source zones of the remaining tsunamis are Andaman-Nicobar islands, Burma-Bangladesh region in the eastern side, and Makran subduction zone in the west. Similar to Dominey-Howes et al. (2006) [7], they reported 3 paleotsunamis in the Makran subduction zone. Also, their investigation shows that Makran subduction zone has produced the deadliest tsunami in the Indian Ocean prior to 2004 mega-tsunami, i.e. 1945 tsunami. Considering above-mentioned facts, Sunda and Makran subduction zones are the most tsunamigenic regions in the Indian Ocean and the first priority should be given to the assessment of tsunami hazards in these zones.

Iran is one of the Indian Ocean countries,

which is at risk of tsunami on its southern coasts from Makran subduction zone. The Makran subduction zone, with more than 900 km in length, is located off the southern coasts of Iran and Pakistan in the north-western Indian Ocean. In this region the Oman oceanic lithosphere slips below the Iranian micro-plate at the estimated rate of about 19 mm/yr [8].

The last major historical earthquake and tsunami in the MSZ occurred on 28 November 1945 at 21:56 local time. The epicenter of the earthquake was located at latitude 24.50 ºN and longitude 63.00 ºE, about 87.1 kilometers from the south west of Churi, Pakistan. The magnitude of the earthquake was evaluated to be 8.1. In fact, this was the last major tsunami-generating earthquake in the Makran zone. The destructive tsunami killed more than 4,000 people and caused great loss of life and devastation along the coasts of Western India, Iran, Oman and Pakistan [9 and 10]. Based on the above-mentioned facts, the risk of tsunami in southern coasts of Iran bordering the Indian Ocean is relatively high and it is necessary to evaluate the hazard of tsunami and to establish a tsunami warning system. Since tsunamis are generated by abrupt vertical deformation of ocean floor, the pattern and extent of vertical ground deformation from an earthquake determines the strength of associated tsunami. In fact, the larger the magnitude of an earthquake, the larger the area that is deformed, and consequently, the stronger the tsunami produced [1]. Hence, to assess the possibility of tsunami generation in a particular region, in the first step it is necessary to simulate the size and distribution of seafloor deformation after the earthquake occurrence.
In the framework of this study, a computer program is developed based on Mansinha and Smylie (1971) [11] formula to predict the seafloor deformation due to the earthquake occurrence in the subduction zone. At first, the model was verified through run of the model on some actual tsunamis so far occurred. Subsequently, considering data of the Makran 1945 tsunami, the seismic parameters of the Makran subduction zone were calibrated. Finally, we used the developed computer program to calculate seafloor deformation at the location of Makran subduction zone for several earthquake scenarios with moment magnitudes ranging between 6.5 and 8.5. At the end of the paper, based on the calculated seafloor deformation, the possibility for tsunami generation in the southern coasts of Iran is discussed.

2. Short Review of Related Research Works

Considering unusual loss of life and damages caused by tsunami, the problem of tsunami hazard has been investigated for various vulnerable coastlines to the impact of tsunami throughout the world. In the following paragraphs some of these efforts are mentioned.

Legg et al. (2004) [12] investigated the tsunami hazard associated with the Catalina Fault offshore of southern California. They used realistic faulting parameters and employed several earthquake scenarios with moment magnitudes ranging between 7.0 and 7.6 as initial conditions for tsunami hazard assessment in southern California.

Rikitake and Aida (1988) [13] studied the tsunami hazard probability in Japan. They evaluated probability of the tsunami-generating earthquake occurring during 2000 to 2010 either from historical data of earthquake occurrence or from near-shore

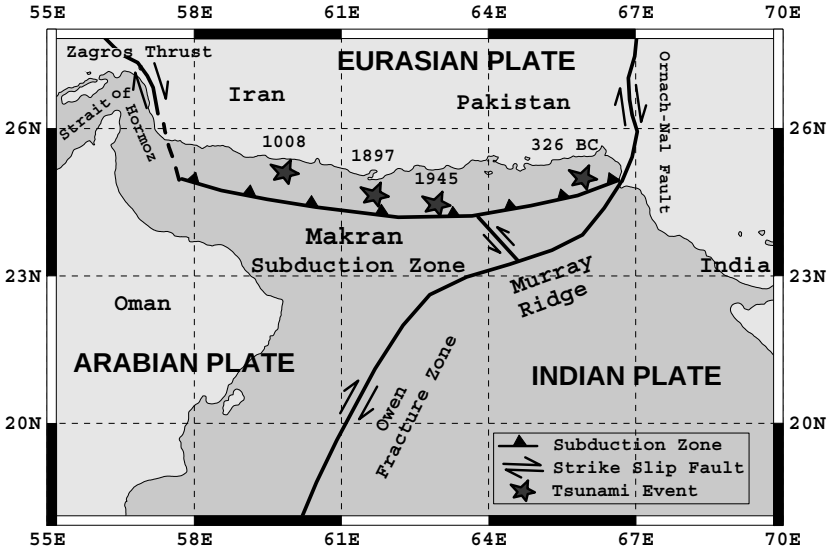

Fig.3 Tectonic map of the Arabian, Indian and Eurasian plates showing the location of the Makran subduction zone. Also, the locations of Makran historical tsunamis are specified by red stars.

crustal strain accumulation.

Hebert et al. (2004) [14] investigated the tsunami hazard in the Marmara Sea. At first, they summarized the historical records of tsunami occurrences in the Marmara Sea. Then, they determined the most tsunamigenic sources in the Sea of Marmara and calculated the probable earthquake from each zone. Finally, they evaluated the potential for tsunami generation from each tsunamigenic source.

Pelinovsky et al. (2001) [15] discussed the problem of tsunami-risk for the French coast of the Mediterranean. They described and analyzed historical data of tsunami manifestation on the French coast. Based on historical data of earthquake and tsunami occurrences, they found that the average value of tsunamigenic earthquake in this region is about 6.8. Then, they extracted a mathematical relation between earthquake magnitude and rupture length.

Tinti and Armigliato (2003) [16] evaluated the hazard of tsunami in southern Italy using different scenarios. They considered three different scenarios for tsunamigenic zone and using seismic parameters of each zone, they evaluated the potential for tsunami generation from each source.

As can be seen, for tsunami hazard assessment in any particular region at first the historical records of tsunami occurrences in that region should be investigated. Then, the potential for tsunami generation in the given tsunamigenic source should be evaluated considering the seismic characteristics of the tsunamigenic source.

3. Tectonic Setting of Makran Subduction Zone

The Makran subduction zone is located in the southwestern part of Pakistan and southeastern Iran with the length of approximately 1000 km from near Karachi to the Straits of Hormuz (Figure 3). The Makran zone results from the convergence between the Arabian plate with the Eurasian plate. In this region the Oman oceanic lithosphere

slips below the Iranian micro-plate.

Makran is characterized by extremely shallow subduction angle [17]. Analysis of seismic parameters of previous Makran earthquakes reveals that their dip angle is about 7 degrees [18].

Byrne et al. (1992) [18] reported that the actual rate of convergence is about 40 mmy-1 on average, increasing from 36.5 mmy-1 in the west Makran to 42 mmy-1 in the east Makran. The mentioned subduction rate was obtained by assuming a completely rigid plate motion.

However, recent studies by employing a network of 27 GPS (Global Position System) in Iran and Northern Oman reveals that the subduction rate at the Makran zone is about 19.5 mmy-1 [8].

The boundaries of the Makran subduction zone are rather complex tectonic areas [18]. As shown in Figure 3, major transparessional strike-slip systems, the Ornach-nal fault zones, form the eastern boundary of Makran zone. On the other hand, the western boundary forms a transition zone between the Zagros continental collision and the Makran Oceanic subduction [8]. Also, Figure 3 shows that to the south the Murry ridge delineate part of the Arabian-Indian plate boundary.

4. Historical Tsunamis in Makran

Data of historical tsunamis in the Indian Ocean basin are collected by some researchers including Murty and Rafiq (1991) [4], Murty and Bapat (1999) [5], Dominey-Howes et al. (2006) [7], and Rastogi and Jaiswal (2006) [6]. According to these catalogs, the total number of tsunami events in the Makran zones is 3, including two events of seismic origin, and 1 of unknown origin. Also, Ambraseys and Melville (1982) [9] investigated the history of earthquake occurrences in Iran, and presented a limited review of tsunami events in southern coasts of Iran. They stated that historically large sea waves have caused sever damages and loss of life along the Makran coasts. Besides above-mentioned 3 tsunamis in the Makran coast, they have reported another tsunami has occurred in this region in 1897, which origin was climatic floods (Figure 3).

Totally, investigation of historical records of tsunami occurrences in the Makran subduction zone demonstrates that 4 tsunamis are reported in Makran zone including the events of 326 BC, 1008, 1897, and 1945. Also, the locations of these events are specified by red stars in Figure 3.

Among Makran historical tsunamis, only the earthquake and tsunami of November 28, 1945 was well documented. This catastrophic earthquake caused significant damage and numerous casualties in all along the Makran coasts, and caused deaths as far as Mumbai [6]. The epicenter of the earthquake with magnitude of 8.1 [18] was located off the southern coasts of Pakistan at 24.50oN, 63.00oE. As mentioned above, the 1945 event in Makran is the secondly deadliest tsunami in the Indian Ocean after the 2004 mega-tsunami, which killed more than 4000 people [6]. The tsunami reached a height of 17m in some Makran ports and caused great damage to the entire coastal region.

5. A Model for Simulation of Seafloor Deformation

Tsunamis are generated by sudden vertical displacement of ocean floor due to

earthquake occurrence in the location of subduction zones. As mentioned before, the pattern and extent of vertical ground deformation from an earthquake uniquely determines whether or not a tsunami is formed [1]. Hence, for tsunami modeling at first, the size and distribution of ocean floor deformation following an undersea earthquake should be calculated.

To address this problem, Steketee (1958) for the first time applied Volterra's formula (equation 1) to the general study of dislocation in an elastic half-space [11].

$$u_i = \int_{\Sigma} \Delta u_j \left[\delta_{jk} \lambda \frac{\partial u_i^l}{\partial \xi_l} + \mu \left(\frac{\partial u_i^j}{\partial \xi_k} + \frac{\partial u_i^k}{\partial \xi_i} \right) \right] \nu_k dS \quad (1)$$

Where the integral is over the dislocation surface, ν_k is the outward normal vector to Σ, μ and λ are the Lame constants, u_i^j is the ith component of displacement at (x_1,x_2,x_3) due to a point force of unit magnitude at $(\zeta_1, \zeta_2,\zeta_3)$ acting in the j-direction, δ_{jk} is the Kronecker delta, and Δu_j is the dislocation across a surface of Σ. Volterra's formula gives the displacement field as an integral over the fault surface involving nuclei of strain which can be interpreted as being due to the action of systems of point forces [11].

After the introduction of dislocation theory to the field of seismology by Steketee (1958), numerous theoretical formulations describing the deformation of an isotropic homogeneous semi-infinite medium have been developed with increasing completeness and generality of source type and geometry.

Mansinha and Smylie (1971) [11] using Volterra's formula developed integral equations for displacement fields of rectangular slip faults. Then, they analytically solved the extracted integral

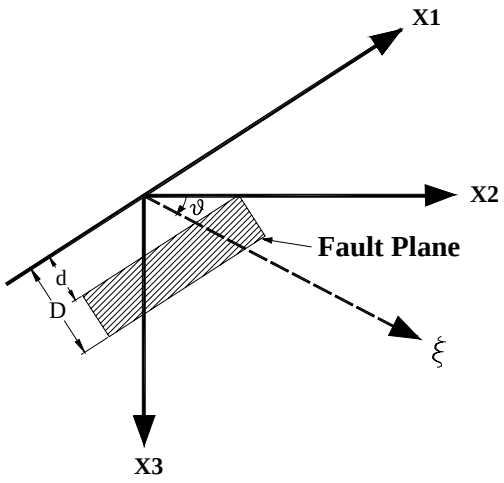

Fig.4 Geometry of fault used in this study

equations and proposed closed analytical expressions for the displacement fields of inclined, finite strike-slip and dip-slip faults. Another similar solution of the Volterra's formula is performed by Okada (1985) [19]. Both solutions use the same algorithm. However, the only difference between them is that the Okada one allows for tensile crack.

Here, the algorithm of Mansinha and Smylie (1971) [11] is used to calculate the seafloor deformation. Mansinha and Smylie (1971) [11] showed that for rectangular slip faults with the geometry shown in Figure 4, for a strike slip fault (slip of magnitude U_1 in x_1 direction) the displacement field will be calculated using equation 2 and for a dip-slip fault (slip of U down fault dip) the displacement field will be calculated using equation 3.

Then, Mansinha and Smylie (1971) [11] integrated equations 2 and 3 over the fault surface . Finally, they obtained closed analytical expressions for surface deformation due to earthquake occurrence. An example of Mansinha and Smylie's (1971) solution is presented in equation 4 which shows the horizontal component of the uplift for strike-slip faults.

$$u_i = \mu U_1 \int_{\Sigma} \left[\left(\frac{\partial u_i^1}{\partial \xi_2} + \frac{\partial u_i^2}{\partial \xi_1} \right) Sin\theta - \left(\frac{\partial u_i^1}{\partial \xi_3} + \frac{\partial u_i^3}{\partial \xi_1} \right) Cos\theta \right] dS \quad (2)$$

$$u_i = \mu U \int_{\Sigma} \left[\left(\frac{\partial u_i^2}{\partial \xi_2} - \frac{\partial u_i^3}{\partial \xi_3} \right) Sin2\theta - \left(\frac{\partial u_i^2}{\partial \xi_3} + \frac{\partial u_i^3}{\partial \xi_2} \right) Cos2\theta \right] dS \quad (3)$$

$$12\pi \frac{u_1}{U_1} = (x_1 - \xi_1) \left[\frac{2r_2}{R(R + r_3 - \xi)} - \frac{4q_2 - 2x_3 \cos\theta}{Q(Q + q_3 + \xi)} - \frac{3\tan\theta}{Q + x_3 + \xi_3} + \frac{4q_2 x_3 Sin\theta}{Q^2} + 4q_2 q_3 x_3 Sin\theta \frac{(2Q + q_3 + \xi)}{Q^2 (Q + q_2 + \xi)^2} \right] - 6\tan^2\theta \tan^{-1} \left[\frac{(k - q_2 Cos\theta)(Q - k) + (q_3 + \xi) k Sin\theta}{(x_1 - \xi_1)(q_3 + \xi) Cos\theta} \right] + 3\tan^{-1} \frac{(x_1 - \xi_1)(r_3 - \xi)}{r_2 R} - 3\tan^{-1} \frac{(x_1 - \xi_1)(q_2 + \xi)}{q_2 Q} \quad (4)$$

In the above equations, U_1 is the magnitude of slip strike slip fault in x_1 direction, U is the magnitude of slip dip slip fault, θ is the dip angle of the fault,and R, Q, r_2, r_3, q_2, and q_3 are defined as follows:

$$R^2 = (x_1 - \zeta_1)^2 + (x_2 - \zeta_2)^2 + (x_3 - \zeta_3)^2 \quad (5)$$

$$Q^2 = (x_1 - \zeta_1)^2 + (x_2 - \zeta_2)^2 + (x_3 + \zeta_3)^2 \quad (6)$$

$$r_2 = x_2 \sin\theta - x_3 \cos\theta \quad (7)$$

$$r_3 = x_2 \cos\theta + x_3 \sin\theta \quad (8)$$

$$q_2 = x_2 \sin\theta + x_3 \cos\theta \quad (9)$$

$$q_3 = -x_2 \cos\theta + x_3 \sin\theta \quad (10)$$

Mansinha and Smylie (1971) [11]'s algorithm is based on input seismic parameters that include the strike (θ_1), dip (θ_2), and slip (θ_3) angles, the amount of slip on the fault surface (D), the dimensions (L and W) of the ruptured area, and the earthquake depth (H). These parameters are shown in Figure 5. Figure 6 presents flowchart of the developed program.

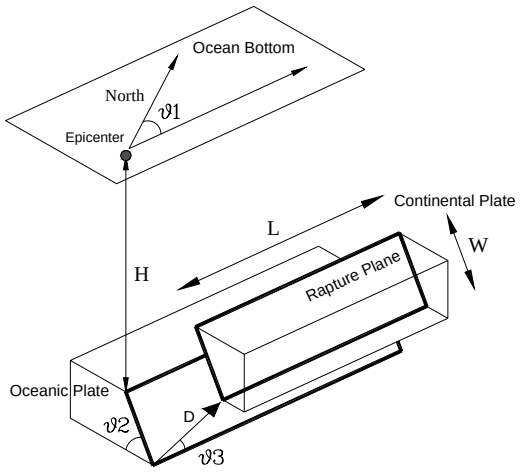

Fig.5 Parameters used for tsunami source modeling

It should be noted that Mansinha and Smylie's (1971) solution was obtained by assuming the earth as uniform elastic half-space. According to Mansinha and Smylie (1971), their equations are valid for calculation of near-field displacement, rather than far-field one, thus the half space assumption is acceptable. In the framework of this study, since we are interested in the modeling of the ocean-floor uplift exactly at the earthquake epicenter, therefore, we calculate the near-field displacement. Hence, our application of the Mansinha and Smylie's (1971) equation is in good agreement with their assumption.

6. Model Verification

A critical part of any scientific modeling effort is model verification or validation in which comparisons between model predictions and actual field data are accomplished.

In this study for verification of the model, we employ the model to calculate seafloor uplift of some actual tsunami events and compare results obtained from the model with actual field data. The tsunami events used in this

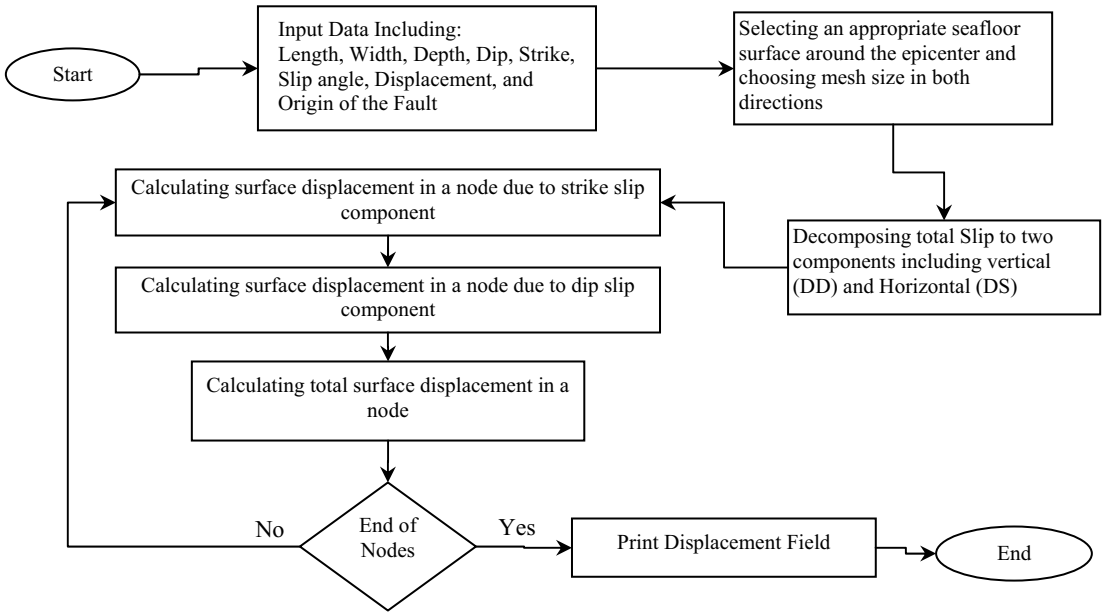

Fig.6 The flowchart of the developed program for simulation of seafloor deformation due to earthquake

Table 1 Comparison of the actual field data and model results for some real tsunami events

Event Name	Quake Magnitude	Rupture (km) Length/Width	Dip/Strike/Slip Angles (Deg)	Depth/Displac. (km)/(m)	Actual Uplift (m)	Model Uplift (m)	Error (%)
Portugal,1969[1]	7.3	80/50	-/55/52	-/3	+1.07	+0.97	-10.3
Portorico,1918[2]	7.3	66/23	70/205/106	4/4	+0.80	+0.73	-9.6
Mexico,1995[3]	8.0	160/60	16/309/90	10/4	+1.85	+1.70	-8.8
Mexico,1962[4]	7.1	40/35	25/296/90	12/0.65	+0.22	+0.24	+9.1
Indonesia,2004[5]	9.3	443/170	8/329/110	25/30	+10.0	+11.11	+11.1

1: Guesmia et al., 1998 [20]; 2: Mercado and McCann, 1998 [21]; 3: Ortiz et al., 2000-a [23]; 4: Ortiz et al., 2000-b [22]; 5: Yalciner et al., 2005 [24].

study for model verification include Portugal 1969 tsunami reported by Guesmia et al. (1998) [20]; Portorico 1918 tsunami reported by Mercado and McCann (1998) [21]; Mexico 1962 tsunami reported by Ortiz et al. (2000-b) [22]; Mexico 1995 tsunami reported by Ortiz et al. (2000-a) [23]; and most recent mega-tsunami of 2004 in Indonesia reported by Yalciner et al. (2005) [24].

Seismic parameters (rupture length, rupture width, dip, strike, and slip angles, epicentral depth, and displacement) of each tsunami event and actual uplift reported from each event are given in Table 1. Based on the seismic parameters of each tsunami event and using the developed model, we calculated the uplift of each event. The predicted uplifts are shown in column 7 of the Table 1. Also, Figure 7 presents a plot of the actual field data and model predictions.

As shown in the last column of Table 1, the average value of error is ranging between -10 and +10 percent. For three cases the actual uplift is larger than model prediction while

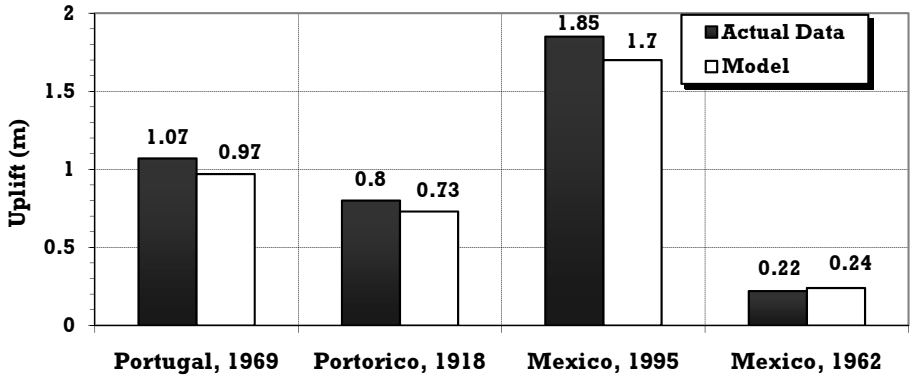

Fig.7 Plot of the actual field data and the model predictions

for other two cases it is smaller than model result. This means that the model is not predicting the seafloor deformation always smaller than actual data or always larger than them.

On the whole, by taking into account the errors in the variables, especially in reported rupture length, width, displacement and other parameters, the observed level of errors associated with the model seems to be in the acceptable range.

7. Calibrating Makran Seismic Parameters

For tsunami hazard assessment, the stage of seafloor deformation calculation always is very important and should be done as accurately as possible because any error in this stage may significantly affect our assessment of the tsunami generation potential. Accurate seafloor deformation modeling depends on the proper selection of the seismic parameters of tsunamigenic zone.

For estimation of seismic parameters of Makran possible earthquakes, details of two main Makran earthquakes are presented in Table 2. Also, empirical relations presented by Wells and Coppersmith (1994) [25] are used to related moment magnitude of earthquake to dimensions of rupture (Length and Width), and displacement (equations 11-13).

$$Log(L) = -3.22 + 0.69M \quad (11)$$

$$Log(W) = -1.01 + 0.32M \quad (12)$$

$$Log(u) = -4.80 + 0.69M \quad (13)$$

where u is the displacement on the fault surface, L and W are fault length and width respectively and M is the earthquake magnitude.

Table 2 Source parameters of the earthquakes of 1945 and 1947 [18]

Event	Depth (km)	Magnitude	Rake (deg)	Dip (deg)	Strike (deg)
1945.11.28	24	8.1	89	7	246
1945.08.05	20	-	68	7	236

In the following paragraphs it is described how each fault parameter is selected.

Strike angle: As shown in figure 3, Makran subduction zone is relatively straight. Therefore, we use only one rectangular source for tsunami generation modeling. In addition, considering Figure 3 and seismic

data presented in Table 1, the strike angle of the possible rupture is approximately 240 degrees.

Dip angle: It was mentioned before that Makran is characterized by shallow subduction angle. Also, analysis of seismic parameters of previous earthquakes presented in Table 2 reveals that their dip is about 7 degrees. In addition, recent seismic reflection profiles across the Makran subduction zone shows that the Makran subduction zone include extremely low dip angle, ranging between 2 to 8 degrees [17 and 26]. Therefore, we consider the dip angle to be in the range of 4 to 8 degrees.

Slip angle: A review of 36 tsunamigenic earthquakes from different subduction zones performed by Polet and Kanamori (2000) [27], shows that the average slip angle (rake) of those events is about 91 degrees. In fact, the dominant source mechanism for subduction zone earthquakes is dip slip. Also, Table 2 shows that the rake of 1945 Makran tsunami was 89 degrees. However, most faults combine both strike and dip motions, hence; the slip angle has been chosen between 90 and 100 degrees.

Earthquake depth: Typical depth of tsunamigenic earthquakes is less than 30 km. Earthquakes deeper than about 30 km rarely cause sufficient deformation to generate tsunamis [1]. The average depth of 36 tsunamigenic earthquakes [27] is about 25 km. In addition, as presented in Table 2, the depth of the Makran 1945 tsunami was 24 km. Regarding these facts, we consider the earthquake depth to be in the range of 20 to 25 km.

Rupture dimension and displacement: In this order, as mentioned before, the empirical relations presented by Wells and Coppersmith (1994) [25] are used.

Calibration: For calibration of our source modeling, the only available information is some limited reports from Makran 1945 tsunami. Ambraseys and Melville (1982) [9] reported 2 m uplift and -1.5 m subsidence during the 1945 Makran earthquake and tsunami (M_w = 8.1, and moment=1.8×10^{21} N.m). Therefore, considering variable values for fault dip, earthquake depth, slip angle, fault width, and fault displacement we try to reproduce the mentioned uplift and subsidence for the case of an Mw 8.1 earthquake in the Makran zone. Each parameter varies in the aforementioned range.

Using empirical relations presented by Wells and Coppersmith (1994) [25], by choosing the earthquake magnitude as 8.1, the rupture length, width, and displacement would be 234 km, 38 km, and 6.15 m respectively. Figures 8 to 12 demonstrates maximum seafloor uplift and subsidence for different values of mentioned parameters. In each figure, only one parameter varies and the other parameters are kept constant.

Figure 8 demonstrate that by increasing the dip angle of the fault, the maximum uplift of the seafloor slightly increases while the maximum subsidence decreases. Figure 9 shows the deeper the hypocenter of an earthquake, the smaller the vertical motion of the seafloor. Based on the Figure 10, it can be concluded that pure dip slip faults (slip angle=90) can produce more vertical displacement than combined faults (slip angle>90). Also, Figures 11 and 12 shows that by increasing the width of the rupture and fault displacement, both uplift and subsidence increase. In addition, it can be inferred from figures 8 to 12 that the effect of earthquake depth and displacement on the

vertical displacement of seafloor is more than other parameters. Among these parameters, fault displacement has the greatest effect on the vertical displacement.

To select final fault parameters, it should be noted that the seismic moment of 1945 earthquake is 1.8×10^{21} N.m [18]. Hence, any variation of rupture dimensions or displacement should satisfy mentioned value. It is well known that for a rectangular fault of length and width, the seismic moment is defined as:

$$M_0 = \mu LWD \qquad (14)$$

in which, D is the fault displacement, and μ is the rigidity of earth and is in the order of 5×10^{10} Nm^{-2}. Regarding information obtained from Figures 8 to 12, and keeping in mind the seismic moment of 1.8×10^{21} N.m, we select 4 different scenarios in order to reproduce 2 m uplift and -1.5 m subsidence for the 1945 event.

Figure 8 demonstrates that maximum subsidence is inversely proportional to the fault dip, i.e. to increase maximum subsidence; the fault dip should be decreased. Hence, to produce -1.5 m subsidence, we choose fault dip in the range of 5 and 5.5 degrees.

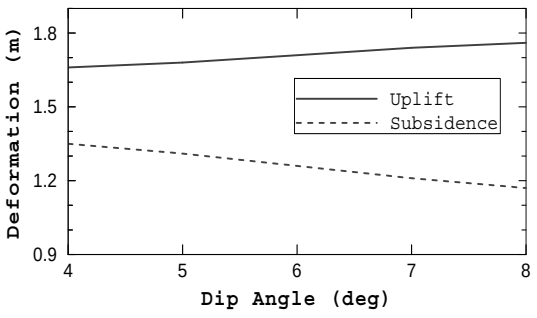

Fig.8 Maximum seafloor uplift and subsidence for different values of fault dip (Depth=20 km, Slip Angle=90 deg, Displacement=6.15 m and Width=38 km)

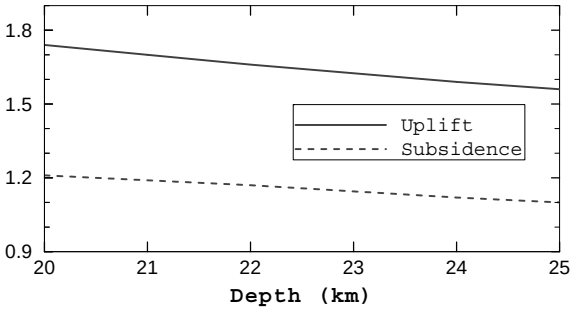

Fig.9 Maximum seafloor uplift and subsidence for different values of depth (Dip=7 deg, Slip Angle=90 deg, Displacement=6.15 m and Width=38 km)

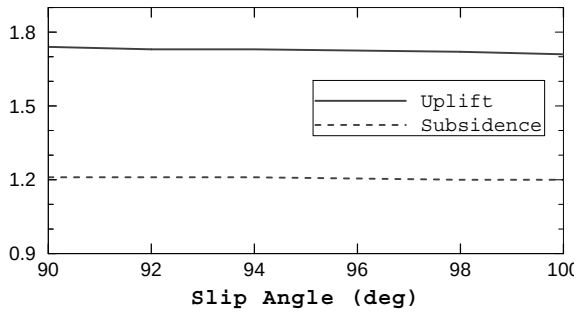

Fig.10 Maximum seafloor uplift and subsidence for different values of slip angle (Depth=20 km, and Dip=7 deg, Displacement=6.15 m and Width=38 km)

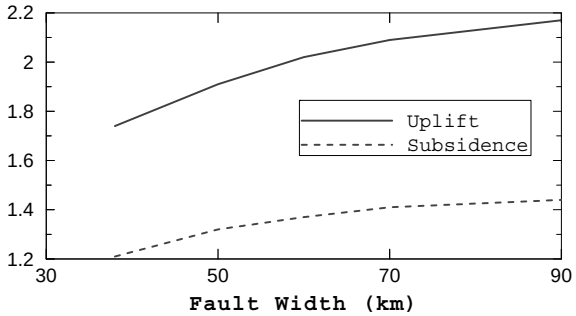

Fig.11 Maximum seafloor uplift and subsidence for different values of fault width (Depth=20 km, Dip=7 deg, Slip Angle=90 deg and Displacement=6.15 m)

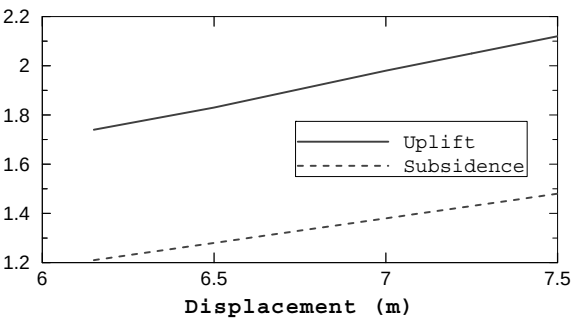

Fig.12 Maximum seafloor uplift and subsidence for different values of fault displacement (Depth=20 km, Dip=7 deg, Slip Angle=90 deg and Width=38 km)

Table 3 Four source scenarios considered in order to reproduce 2 m uplift and 1.5 m subsidence for the case of an Mw 8.1 earthquake in the Makran zone

No.	Dip (deg)	Slip Angle (deg)	Strike (deg)	Depth (km)	Length (km)	Width (km)	Displacement (m)	Moment (Nm)	Maximum Uplift (m)	Maximum Sub. (m)
1	5	90	240	20	126	38	7.50	$1.8x10^{21}$	2.04	-1.56
2	5	90	240	20	128	38	7.40	$1.8x10^{21}$	2.02	-1.54
3	5.5	90	240	20	129	38	7.35	$1.8x10^{21}$	2.02	-1.50
4	5.5	90	240	20	129	38	7.30	$1.8x10^{21}$	**2.01**	**-1.49**

Table 4 Makran source parameters after calibration

Dip Angle (deg)	Slip Angle (deg)	Strike Angle (deg)	Depth (km)	Rupture Length (km)	Rupture Width (km)	Rupture Displacement (m)
5.5	90	240	20	(W. & C. Equ.)* x 0.55	W. & C. Equ.	(W. & C. Equ.)x 1.187

Wells and Coppersmith (1994) [25]'s Equation

These scenarios are presented in Table 3. For each case the maximum uplift and subsidence is calculated. As detailed in Table 3, among 4 source models, the scenario number 4 can reproduce the required vertical displacement very well. It can be inferred from scenario number 4 that for our problem, the empirical relations of Wells and Coppersmith (1994) [25] should be employed with some modifications. In this order, fault length predicted by their equation should be multiplied by 0.55. Also, the displacement is the product of their estimation and 1.187. Finally, Table 4 presents the source parameters after calibration.

8. Application of the Model for Makran Subduction Zone

In this section using the developed program, and after calibration of Makran seismic parameters, we model possible seafloor deformation in the Makran subduction zone due to earthquake occurrence in this tsunamigenic zone. In fact, we use the seafloor deformation as a tool to assess the possibility for tsunami generation.

Several earthquake scenarios with moment magnitudes ranging between 6.5 and 8.5 are used as initial conditions for analysis. Then, using source parameters presented in Table 4, the displacement field of seafloor deformation is calculated for each case-scenario.

As shown in Table 4, for all earthquake scenarios the four parameters including dip angle, slip angle, strike angle, and earthquake depth are constant and do not vary with the earthquake magnitude. In fact, mentioned parameters are inherent characteristics of the tsunamigenic zone and do not depend on the earthquake magnitude. The other three parameters (rupture length, rupture width, and displacement on the fault surface) are direct functions of earthquake magnitude (M).

The results of seafloor deformation modeling for different earthquake scenarios are presented in Table 5. Figure 13 presents 2D in plan view of seafloor deformation at the Makran subduction zone for the case of Mw 8 earthquake. Figure 14 depicts vertical displacement of seafloor along a cross section perpendicular to strike of dislocation through its center for different case-scenarios. The location of this cross section (cross section A-A) is shown in Figure 13. In

Table 5 Results of tsunami generation analysis

Earthquake Magnitude	Rupture Length (km)	Rupture Width (km)	Displacement (m)	Seismic Moment (10^{20}Nm)	Maximum Uplift (m)	Maximum subsidence (m)
6.5	10	12	0.57	0.03	**+0.00**	**-0.00**
6.8	17	15	0.93	0.12	**+0.07**	**-0.05**
7.0	23	17	1.31	0.26	**+0.14**	**-0.10**
7.3	36	21	2.02	0.76	**+0.32**	**-0.23**
7.5	51	25	2.85	1.82	**+0.56**	**-0.41**
7.7	68	28	3.92	3.73	**+0.88**	**-0.65**
8.0	110	35	6.17	11.9	**+1.63**	**-1.20**
8.1	129	38	7.30	17.9	**+2.01**	**-1.49**
8.2	151	41	9.73	30.1	**+2.77**	**-2.05**
8.3	177	44	10.1	39.3	**+2.95**	**-2.20**
8.4	207	48	11.7	58.1	**+3.52**	**-2.62**
8.5	243	51	13.7	84.9	**+4.19**	**-3.13**

addition, a 3D view of seafloor deformation is presented in Figure 15 for the case of Mw 8 earthquake.

9. Discussion

Figure 1, Figures 13, 14, and 15 demonstrate that the seafloor deformation at the location of Makran subduction zone consists of a zone of subsidence towards coastline and an uplift zone towards open ocean.

Regarding Table 5, our source modeling reveals that earthquake having moment magnitude less than 7.5; do not generate sufficient vertical displacement on the ocean floor. Therefore, such earthquakes appear not to generate tsunamis. Figure 16 presents variation of maximum seafloor uplift and subsidence versus different values of earthquake magnitude. This Figure shows that there is an exponential relation between seafloor vertical displacement and earthquake magnitude. As shown, while the vertical deformation is relatively small for earthquake magnitudes up to 7.5, it rapidly increases after that value. This fact indicates that typically, tsunamigenic earthquakes in the Makran subduction zone take the magnitude of more than 7.5. As evidence for this fact, the 1945 Makran tsunami was produced by an Mw 8.1 earthquake.

As can be inferred from Table 1, for earthquake scenarios with magnitude greater than 7.5, the maximum seafloor uplift is considerable indicating high possibility for tsunami generation in the Makran region. In fact, as discussed before, by increasing the vertical seafloor deformation greater volume of the ocean water will be displaced and consequently, stronger tsunami will be produced.

Results obtained here show that the risk of tsunami generation from Makran subduction zone can be classified into three main categories, as follows:

- very little risk for tsunami generation in the case of occurrence of an earthquake having magnitude up to 7;
- little to medium risk for moment magnitudes ranging between 7 and 7.5; and
- high risk for moment magnitude greater than 7.5.

Our analyses of possible seafloor deformation along with historical records of tsunami occurrences in the Makran subduction zone reveal that the risk of tsunami in this region is relatively high and it is necessary to develop a tsunami warning

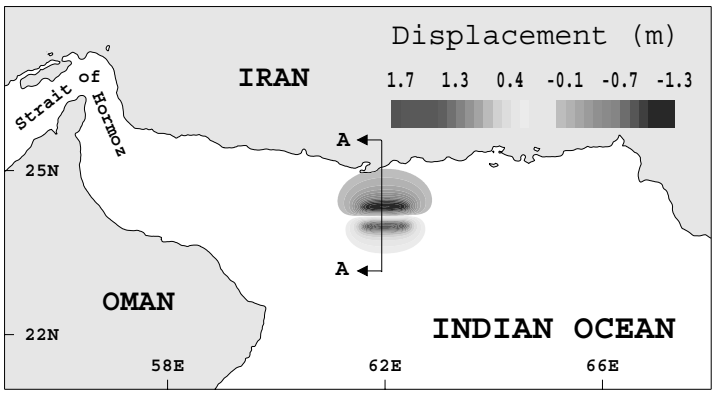

Fig.13 A 2D in plan view of seafloor deformation for the case of M_w 8 earthquake in Makran zone

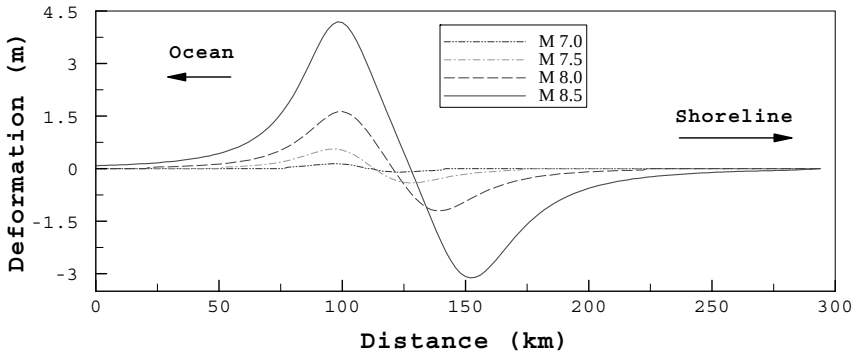

Fig.14 Vertical displacement of seafloor along a cross section perpendicular to strike of dislocation through its center for different cases (along cross section A-A)

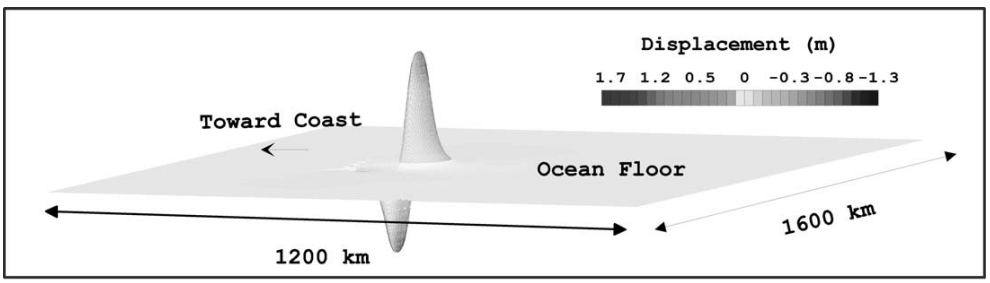

Fig.15 A 3D view of seafloor deformation for the case of Mw 8 earthquake in Makran zone

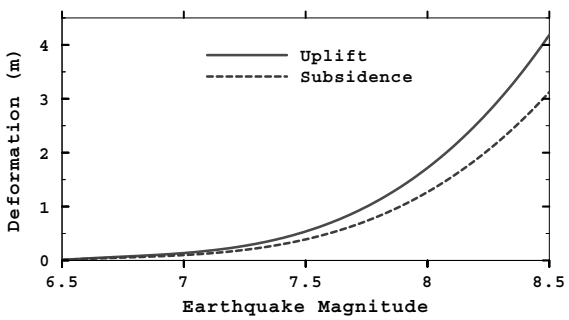

Fig.16 Variation of maximum seafloor uplift and subsidence versus different values of earthquake magnitude

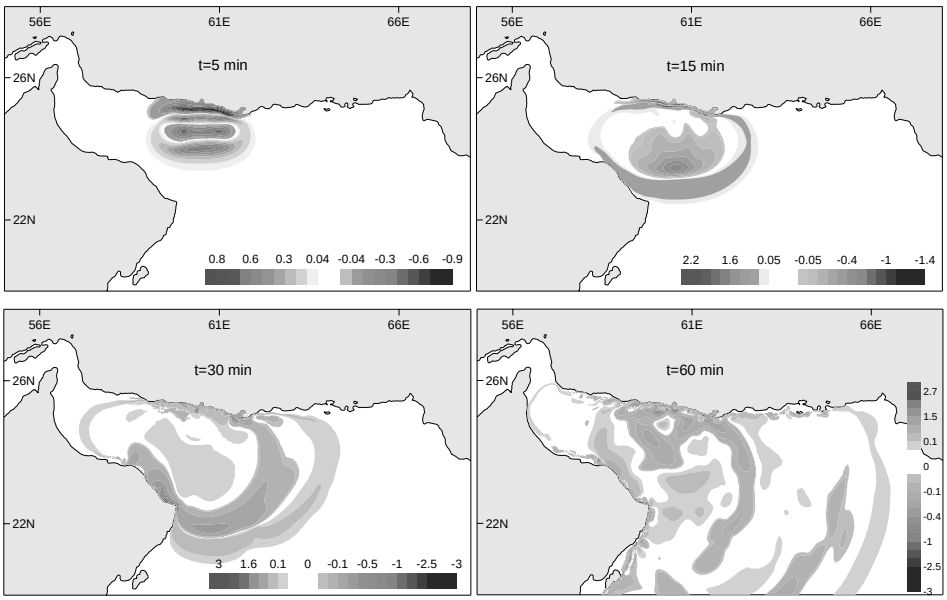

Fig.17 Results of the modeling of tsunami propagation for the case of an earthquake with magnitude 8 offshore Chabahar.

system in this region.

Based on the above-mentioned classification, three different levels of actions should be taken as follows:

M<7: No tsunami warning should be issued.
7<M<7.5: The tsunami warning center should watch and check other data like sea level information and if necessary the warning should be issued.
M>7.5: The tsunami warning should be issued.

10. Modeling of the Tsunami Propagation in the Makran

Since tsunami wavelengths (hundred of kilometers) are much larger than the ocean depth (a few kilometers), tsunamis are considered as shallow water waves, following the long wave theory [28 and 14]. Here, for modeling of tsunami, we employ the method developed by Goto et al. (1997) [28]. Based on the long wave theory, Goto et al. (1997) developed a numerical model for modeling of tsunami propagation. In this study, we use their model for modeling of tsunami propagation.

To investigate the pattern of tsunami propagation in the Makran region, we consider an earthquake scenario with magnitude of 8 whose epicenter lies at 24.5°N and 60.5°E.
At first, we model the seafloor deformation due to this earthquake scenario using the developed computer program in this study. Then, we use the ocean-floor displacement field as the initial condition for tsunami propagation modeling. The results of propagation modeling are presented in Figure 17. This figure includes rather useful information about behavior of tsunami in the Makran subduction zone.

The first piece of information obtained from Figure 17 is that any tsunami in the Makran will hit the nearest coastline within about 15 to 20 minutes.

Also, Figure 17 shows that after about 1 hr, the tsunami will hit all countries in the region

including Iran, Oman, Pakistan and India. For the case of an earthquake scenario with magnitude of 8, the tsunami waves reach the maximum value of about 3 m in the coastal areas. It is evident that by increasing the magnitude of the earthquake, the maximum seafloor uplift will be increased which itself results in higher wave heights at the coastlines.

11. Conclusions

The main findings of this paper can be summarized as follows:

- Assessment of the historical records of tsunamis in the Indian Ocean shows that essentially there are two main tsunamigenic zones in this ocean, which are Sunda subduction zone in the east, and Makran subduction zone in the north-west of the Indian Ocean.

- According to our review of historical earthquakes and tsunamis in the Indian Ocean basin, the total number of tsunami events in the Makran subduction zone is 4, which are: events of 326 BC, 1897, 1008, and 1945.

- To model possibility for tsunami generation in Makran zone, a computer program is developed. The model was verified through run of the model on some actual tsunamis so far occurred. Subsequently, considering data of the Makran 1945 tsunami, the seismic parameters of the Makran subduction zone were calibrated. Finally, we used the developed computer program to calculate seafloor deformation at the location of Makran subduction zone for several earthquake scenarios with moment magnitudes ranging between 6.5 and 8.5.

-Results of tsunami generation modeling reveals that the risk of tsunami generation from Makran subduction zone can be classified into three main categories, as follows: (1) very little risk for tsunami generation in the case of occurrence of an earthquake having magnitude up to 7; (2) little to medium risk for moment magnitudes ranging between 7 and 7.5; and (3) high risk for moment magnitude greater than 7.5.

- Based on our analyses of possible seafloor deformation and considering historical records of tsunami occurrences in the Makran subduction zone, the necessity for development of a tsunami warning system in this region was emphasized.

- An example of tsunami propagation modeling for the case of an earthquake scenario with magnitude of 8 in the Makran region, reveals that the first tsunami wave will hit the nearest coastline within about 15 to 20 minutes and reaches the height of up to 3 m.

12. Acknowledgments

Financial support from Faculty of Engineering of the University of Tehran is acknowledged. Also, the first author would like to extend his sincere gratitude to Prof. Costas E. Synolakis, University of Southern California, California, USA, Prof. Emile A. Okal, Northwestern University, Illinois, USA, and Prof. Ahmet C. Yalciner, Middle East Technical University, Ankara, Turkey, for their helps and discussions throughout his Ph.D. thesis.

13. References

[1] Synolakis C.E., 2003. Tsunami and Seiche. In Earthquake Engineering Handbook, edited by Chen W. F., and

Scawthorn, C., CRC Press: 9–1-9–90

[2] Gusiakov V.K., 2005. Tsunami generation potential of different tsunamigenic regions in the Pacific. Marine Geology, 215: 3 – 9

[3] Gusiakov V. K., 2001. Basic Pacific Tsunami Catalog and Database, 47 BC-2000 AD: Results of the First Stage of the Project. Proceedings of ITS 2001, Session 1, Number 1-2

[4] Murty T., and Rafiq M., 1991. A tentative list of tsunamis in the marginal seas of the north Indian Ocean. Nat. Hazards, 4: 81–83

[5] Murty T., and Bapat A., 1999. Tsunamis on the coastlines of India. Science of Tsunami Hazards, 17(3):167–172

[6] Rastogi B. K., and Jaiswal R. K., 2006. A Catalog of Tsunamis in the Indian Ocean. Science of Tsunami Hazard, 25 (3):128–143

[7] Dominey-Howes D., Cummins P., and Burbidge D., 2006. Historic records of teletsunami in the Indian Ocean and insights from numerical modeling. Nat. Hazards, DOI 10.1007/s11069-006-9042-9

[8] Vernant Ph., Nilforoushan F., Hatzfeld D., Abbasi M. R., Vigny C., Masson F., Nankali H., Martinod J., Ashtiani A., Bayer R., Tavakoli F., and Chery J., 2004. Present-Day Crustal Deformation and Plate Kinematics in the Middle East Constrained by GPS Measurements in Iran and Northern Oman. Geophys. J. Int., 157: 381-398

[9] Ambraseys N. N. and Melville C. P., 1982. A History of Persian Earthquakes. Cambridge University Press, Britain

[10] Carayannis G. P., 2006. The Potential of Tsunami Generation along the Makran Subduction Zone in Northern Arabian Sea. Case Study: The Earthquake and Tsunami of November 28, 1945. Science of Tsunami Hazards, 24(5):358–384

[11] Mansinha L., and Smylie D. E., 1971. The Displacement Field of Inclined Faults. Bulletin of Seismological Society of America, 6: 1433–1440

[12] Legg M. R., Borrero J. C., Synolakis C. E., 2004. Tsunami Hazards Associated with the Catalina Fault in Southern California. Earthquake Spectra, 20(3): 1–34

[13] Rikitake T., and Aida I., 1988. Tsunami Hazard Probability in Japan. Bulletin of the Seismological Society of America, 78 (3): 1268-1278

[14] Hebert H., Schindele F., Altinokb Y., Alpar B., Gazioglu C., 2004. Tsunami Hazard in the Marmara Sea (Turkey)-a Numerical Approach to Discuss Active Faulting and Impacts on the Istanbul Coastal Areas. Marine Geology

[15] Pelinovsky E., Kharif C., Riabov I., and Marcfrancius, 2002. Modelling of Tsunami Propagation in the Vicinity of the French Coast of the Meditranean. Natural Hazards, 25: 135-159

[16] Tinti S. and Armigliato A., 2003. The Use of Scenarios to Evaluate the

Tsunami Impact in Southern Italy. Marine Geology, 199: 221-243

[17] Koppa C., Fruehn J., Flueh E.R., Reichert C., Kukowski N., Bialas J., and Klaeschen D., 2000. Structure of the Makran subduction zone from wide-angle and refleection seismic data, Tectonophysics, 329: 171-191

[18] Byrne D. E., Sykes L. R., Davis D. M., 1992. Great Thrust Earthquakes and Aseismic Slip along the Plate Boundary of the Makran Subduction Zone. Journal of Geophysical Research, 97 (B1): 449–478

[19] Okada Y., 1985. Surface Deformation Due to Shear and Tensile Faults in a Half Space. Bulletin of Seismological Society of America, 75(4): 1135–1154

[20] Guesmia M., Heinrich PH., and Mariotti C., 1998. Numerical Simulation of the 1969 Portuguese Tsunami by a Finite Element Method. Natural Hazards, 17: 31–46

[21] Mercado A., and McCann W., 1998. Numerical Simulation of 1918 Porto Rico Tsunami. Natural Hazards, 18: 57-76

[22] Ortiz M., Singh S. K., Kostoglodov V. and Pacheco J., 2000-b. Source Areas of the Acapulco-San Marcos, Mexico Earthquakes of 1962 (M 7.1; 7.0) and 1957 (M 7.7), as Constrained by Tsunami and Uplift Records. Geofísica Internacional, 39 (4): 337-348

[23] Ortiz M., Kostoglodov V., Singh S. K. and Pacheco J., 2000-a. New Constraints on the Uplift of October 9, 1995 Jalisco-Colima Earthquake (Mw 8) Based on the Analysis of Tsunami Records at Manzanillo and Navidad, Mexico. Geofísica International, 39 (4): 349-357

[24] Yalciner A. C., Karakus H., Ozer C. and Ozyurt G., 2005. Short Course on Understanding the Generation, Propagation, Near and Far- Field Impacts of Tsunamis and Planning Strategies to Prepare for Future Events. MACRES, Malaysia

[25] Wells D. L. and Coppersmith K. J., 1994. New Empirical Relationships among Magnitude, Rupture Length, Rupture Width, Rupture Area, and Surface Displacement. Bulletin of the Seismological Society of America, 84 (4): 974-1002

[26] Schluter H. U., Prexl A., Gaedicke Ch., Roeser H., Reichert Ch., Meyer H., and Daniels C. von, 2002. The Makran accretionary wedge: sediment thicknesses and ages and the origin of mud volcanoes, Marine Geology, 185: 219-232

[27] Polet J., and Kanamori H., 2000. Shallow Subduction Zone Earthquakes and Their Tsunamigenic Potential. Geophys. J. Int., 142: 684-70

[28] Goto C., Ogawa Y., Shuto N., Imamura F., 1997. Numerical method of tsunami simulation with the leap-frog scheme (IUGG/IOC Time Project), IOC Manual, UNESCO, No. 35